Separation and Purification Technology xxx (xxxx) 130943

Contents lists available at ScienceDirect

Separation and Purification Technology

journal homepage: www.elsevier.com/locate/seppur

A novel almond shell biochar modified with FeS and chitosan as adsorbents for mitigation of heavy metals from water and soil

Penghui Guo [a], Xiang Gu [a], Zhaoshuang Li [a,*], Xu Xu [b], Yini Cao [a,c,*], Guoen Yang [a], Chuntao Kuang [a], Xingong Li [a], Yan Qing [a], Yiqiang Wu [a,*]

[a] College of Materials Science and Engineering, Central South University of Forestry & Technology, Hunan Province Key Laboratory of Materials Surface/Interface Science & Technology, Changsha 410004, China

[b] International Innovation Center for Forest Chemicals and Materials, Nanjing Forestry University, Nanjing 210037, China

[c] National Engineering Laboratory for Applied Technology of Forestry & Ecology in South China, Faculty of Life Science and Technology, Central South University of Forestry and Technology, Changsha, Hunan 410004, China

ARTICLE INFO

Editor: Gaohong He

Keywords:
Almond shell
Biochar
Adsorption
Chitosan
Heavy metals

ABSTRACT

The discharge of heavy metals (HMS) from industrial production has severely damaged the natural environment and human health. To address the challenges posed by heavy metals, a novel almond shell biochar (FeS-CTS@nBC) modified with FeS and chitosan (CTS) was prepared. Scanning electron microscopy and X-ray photoelectron spectroscopy observations revealed a uniform distribution of FeS particles on the biochar. Adsorption thermodynamics experiments showed that the maximum adsorbed amounts of cadmium (Cd), lead (Pb), and chromium (Cr (VI) and Cr (III)) in FeS-CTS@nBC were 85.6, 89.63, 94.2, and 75.62 mg/g, respectively. Results of soil incubation experiments indicated that FeS-CTS@nBC had a desirable immobilization effect on heavy metals, decreasing the bioavailability of Cd, Pb, Cr (VI), and Cr (III) by 29.43 %, 23.93 %, 5.75 % and 5.23 %, respectively. Density functional theory (DFT) calculations, revealed that the oxygen-containing functional groups on the biochar exhibited stronger adsorption capacities for heavy metals. Plant potting experiments indicated that the paddy grew well in the soil remediated with FeS-CTS@nBC. The Cd content in the roots and leaves of the paddy after nBCS2 repair was reduced by 28.01 % and 55.73 %, respectively. Overall, this work provides a promising low-cost method with a simple production process for mitigation of heavy metals from water and soil.

1. Introduction

Heavy-metal contamination of water and soil has become increasingly serious with industrial development [1]. Heavy metals have high biotoxicity and persistence, and are easily bioaccumulated. They have been shown to pollute the natural environment and seriously endanger human health [2,3]. Cadmium (Cd (II)), lead (Pb (II)) and chromium (Cr (VI) and Cr (III)) are recognized as major heavy-metal pollutants by several organizations [4,5]. These three heavy metals have higher environmental concentrations than Hg and As. Moreover, they are more toxic to the environment than Zn, Cu, and Ni. These heavy metals are easily accumulated in paddy fields and enter the human body via the food chain [6]. Cd, Pb, and Cr can enter the human body through various pathways, including food, water, dermal contact, and the respiratory system, which increases the risk of exposure [7]. These issues, necessitate the development of methods for the removal of heavy metals [8]. Currently, adsorption, ion exchange, membrane separation, chemical precipitation, and other techniques are the primary methods for the removal heavy metals [9,10]. However, membrane separation technology is costly and complicated to operate [11]. Chemical precipitation produces large volumes of wastewater, which causes secondary environmental pollution [12,13]. Among these methods, adsorption technology has attracted considerable attention because it is inexpensive, environmentally friendly, and has a high removal efficacy [14]. Biochar is considered to be an ideal material as adsorbents for mitigation of heavy metals from water and soil.

Biochar is a carbon rich material, derived from biomass via pyrolysis. Biochar is an adsorbent material with abundant pores, which makes it suitable for the adsorption of heavy metals [15,16]. Compared with other adsorbents, biochar has the advantages of simple preparation, low cost and environmental friendliness [17]. The porous structure of biochar provides a higher adsorption capacity and faster adsorption

* Corresponding authors at: College of Materials Science and Engineering, Central South University of Forestry & Technology, Hunan Province Key Laboratory of Materials Surface/Interface Science & Technology, Changsha 410004, China (Y. Cao).

E-mail addresses: lzs0829@csuft.edu.cn (Z. Li), CherieCYN@163.com (Y. Cao), wuyq0506@126.com (Y. Wu).

https://doi.org/10.1016/j.seppur.2024.130943
Received 27 August 2024; Received in revised form 24 November 2024; Accepted 3 December 2024
1383-5866/

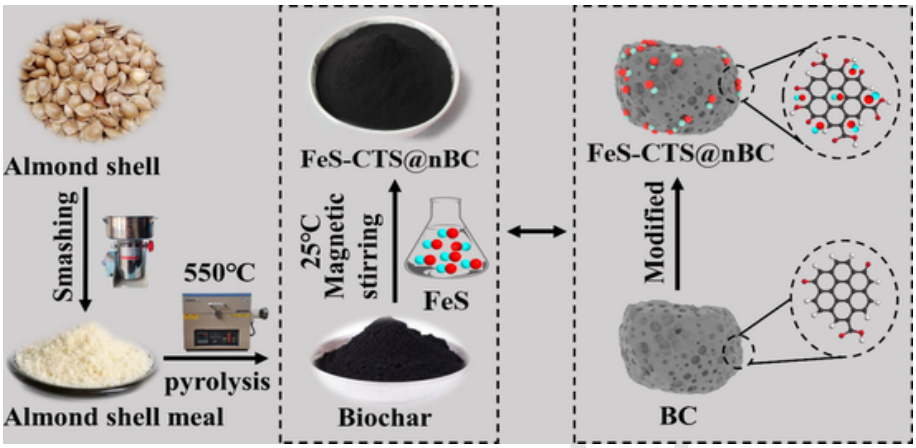

Scheme 1. Preparation process of FeS chitosan-modified biochar.

equilibrium rate, and shows excellent performance in treating pollutants [18]. Additionally, biochar significantly affects the adsorption of pollutants, such as heavy metals and methane [19]. Currently, the materials used for the preparation of biochar include tree branches, straw and nut shells [20,21]. Compared to straw, almond shells have a higher lignin content, which leads to a higher carbon content and facilitates the introduction of oxygen-containing functional groups. The high carbon and low nitrogen contents of almond shells improve the quality of biochar and reduce the emission of nitrogen oxides during carbonization [22,23]. Among nutshells, coconut shell, almond shell, and peach kernel are commonly used for the preparation of biochar [24,25]. In addition, the porous structure of almond shell biochar provides more sites for heavy-metal fixation [26]. Converting almond shells into biochar can realize the resourceful utilization of waste and promote the development of a circular economy. However, unmodified almond shell biochar relies on pore filling to remove heavy metals, which limits its adsorption capacity. Furthermore, its efficiency is easily affected by factors such as temperature and ionic strength [27].

Therefore, this study focused on exploring modification methods to improve the capacity of biochar to remove heavy metals. In recent years, numerous studies have been conducted on biochar modification, including chemical, physical, nanomaterial, and composite modifications [28,29]. Chemical modification improves the adsorption performance of almond shell biochar but often generates toxic by-products and causes secondary environmental pollution [30]. Physical modifications such as ultrasonic and ball-milling treatments can produce biochar with poor stability [31]. Currently, many biochar modifications are composite modifications incorporating nanomaterials [32]. Composite modifications using nanomaterials can improve the stability of biochar and enhance its heavy-metal adsorption capacity [33,34]. The loading of nano-metal ions onto biochar can be used to remove heavy metals through metal-ion reduction and ion-exchange processes [35,36]. Among all the possible materials, nano-FeS is particularly promising for biochar modification. Nano-FeS is a low-cost and highly reducing material, that has been applied in many fields, such as the removal of heavy metals and organic pollutants [37,38]. Furthermore, FeS provides more binding sites than other materials [39]. However, FeS overloading can lead to its accumulation in biochar, limiting the reducing properties of FeS.

In this study, a novel almond shell biochar (FeS-CTS@nBC) modified with FeS, chitosan (CTS), and ball milling was prepared. CTS was added during the modification process to homogeneously disperse FeS and improve its stability. FeS-CTS@nBC was evaluated using scanning electron microscopy (SEM), Fourier transform infrared spectroscopy (FTIR), X-ray photoelectron spectroscopy (XPS), and X-ray diffraction (XRD). The maximum heavy-metal adsorption capacity of FeS-CTS@nBC was explored using metal adsorption experiments. Periodic soil remediation experiments were also conducted. Density functional theory (DFT) is a computational method based on quantum mechanics that is used to study the properties of electronic systems. DFT can efficiently and accurately predict the interactions between biochar surfaces and target molecules to analyze the adsorption performance of biochar [40]. Based on DFT, the effect of increased functional groups on the ability of biochar to adsorb heavy metals was investigated. In addition, paddy potting experiments showed that FeS-CTS@nBC promoted the growth of the paddy fields. Overall, FeS-CTS@nBC is an economical and practical material for the removal of heavy metals and provides a reference for waste resource utilization.

2. Experimental section

2.1. Materials

All chemicals and reagents used in this study were analytical grade or higher. Chemicals such as ferrous sulfate heptahydrate ($FeSO_4$-$7H_2O$, purity ≥ 99.0 %), sodium sulfide hydrate (Na_2S-$9H_2O$, purity ≥ 99.0 %), cadmium chloride ($CdCl_2$, purity ≥ 99.0 %), lead nitrate ($Pb(NO_3)_2$, purity ≥ 99.0 %), potassium dichromate ($K_2Cr_2O_7$, purity ≥ 99.0 %), chromium chloride hexahydrate ($CrCl_3$-$6H_2O$, purity ≥ 99.0 %), copper nitrate ($Cu(NO_3)_2$, purity ≥ 99.0 %), and zinc chloride ($ZnCl_2$, purity ≥ 99.0 %) were obtained from Sinopharm Chemical Reagent Corporation (Shanghai, China). CTS $(C_6H_{11}NO_4)_n$ was sourced from Aladdin (Shanghai, China), and deionized water was used for all experiments.

2.2. Preparation of biochar

The almond shells were obtained from Lingshou County, Hebei Province, China. Hebei almond shells were selected because of their abundance, low price, and desirable qualities. They were washed with deionized water and dried at 80°C. The preparation process is illustrated in Scheme 1. The almond shells were crushed into powder and filtered through a 60-mesh sieve. The filtered powder was pyrolyzed at 550°C (rate: 10 °C/min; pyrolysis time: 120 min) and named BC. In a 500 mL three-necked flask, $FeSO_4$-$7H_2O$ was dissolved in deionized water, and then BC, Na_2S-$9H_2O$, and CTS were added sequentially under magnetic stirring. The resulting solid was freeze-dried for 48 h to obtain FeS-CTS@BC. Throughout the preparation process, magnetic stirring was maintained via continuous nitrogen (N_2) purging. The materials prepared by mixing FeS with BC and CTS in different ratios were la-

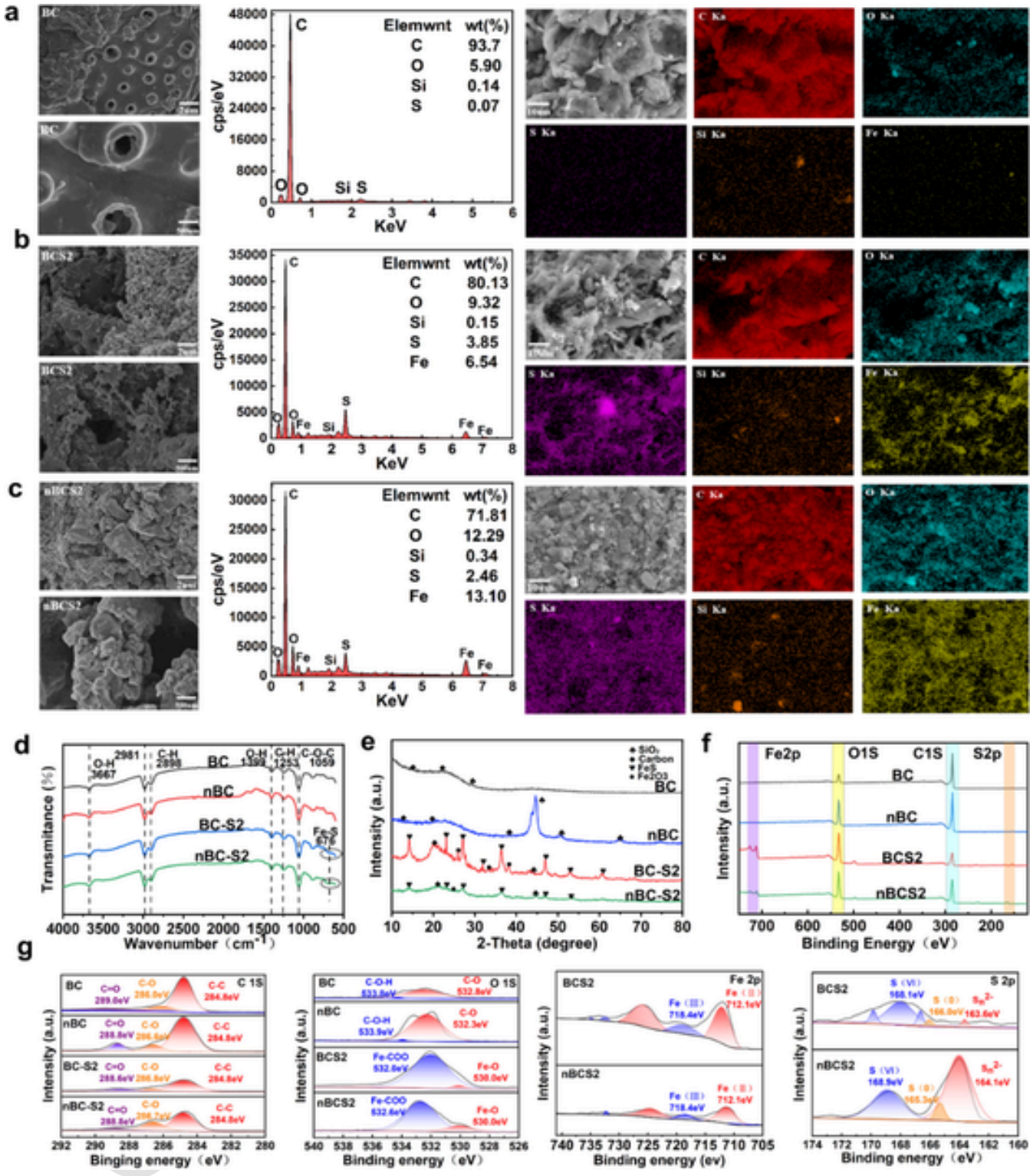

Fig. 1. The Characterization of biochar: SEM images of BC, BCS2 and nBCS2; EDS spectra and elemental mapping of BC (a), BCS2 (b), and nBCS2 (c), FTIR spectra (d), XRD pattern (d), XPS survey spectra (f) with detailed spectra for C1s, O1s, Fe2p and S2p (g).

beled BCS1 (4:1:2), BCS2 (8:1:2), and BCS3 (12:1:2). The modified biochar was further processed via ball milling to prepare FeS-CTS@nBC, which were named nBC, nBCS1, nBCS2 and nBCS3, respectively.

2.3. Characterization of biochar

The surface morphology of biochar was determined using SEM (MIRA 4, TESCAN, Czech). The crystal structure of biochar was determined via XRD (ADVANCE, Bruker, Germany) in the 2θ scanning range of 10° to 80°. The surface functional groups of biochar were observed by

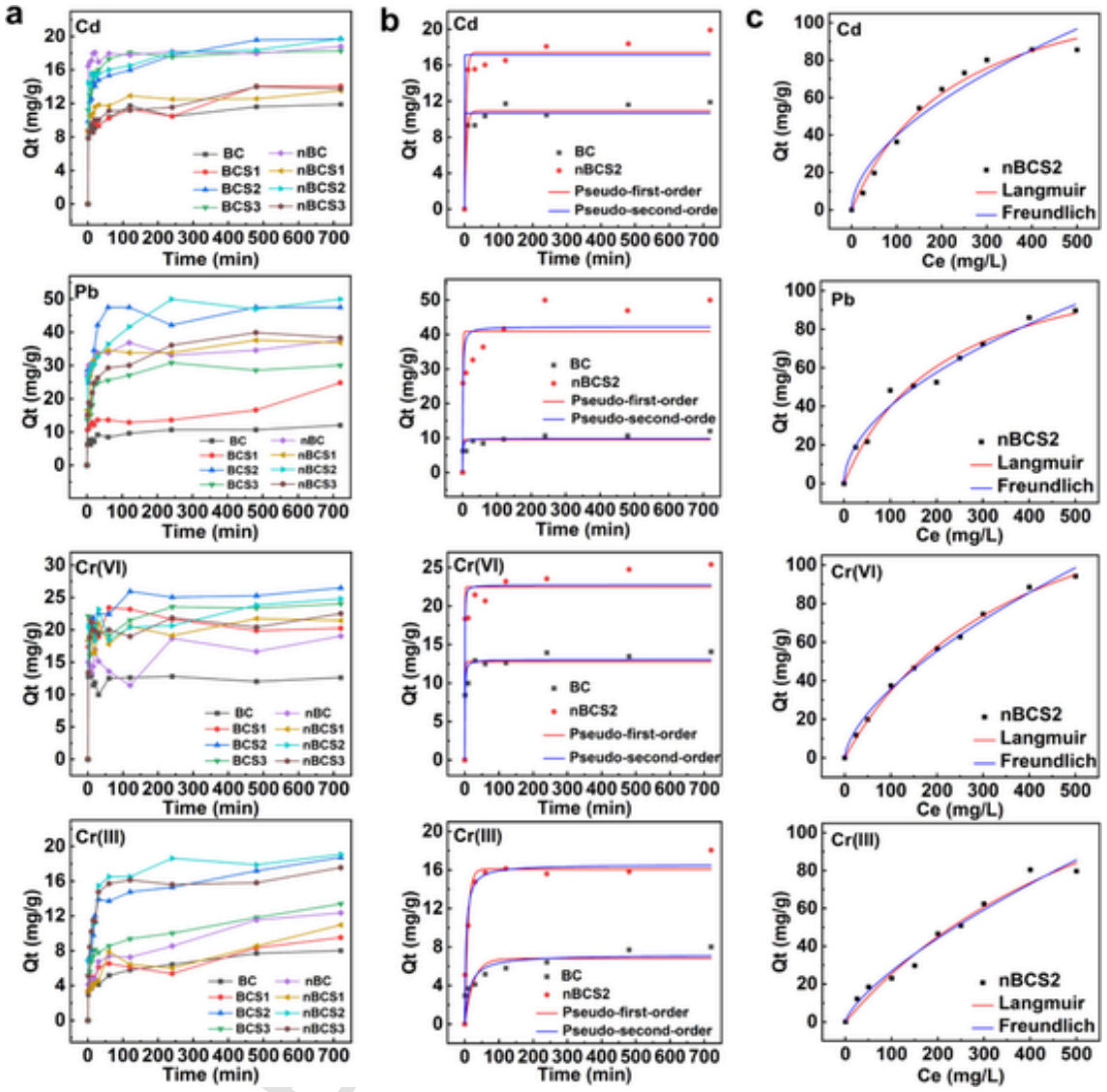

Fig. 2. Removal capacity of biochar for Cd (II), Pb (II), Cr (VI) and Cr (III), dosage: 1 g/L, pH: 5.5, initial concentration: 50 mg/L, temperature: room temperature (a); Kinetics fitting of the Cd (II), Pb (II), Cr (VI) and Cr (III) adsorption on nBCS2 using pseudo-first-order and pseudo-second-order plots (b); Isotherm curve fitting of Cd (II), Pb (II), Cr (VI) and Cr (III) onto nBCS2 fitted by the Langmuir and Freundlich models (c).

FTIR (Was 50 R, Thermo Fisher, USA) with a wave number range of 4000 to 500 cm^{-1}. The elemental composition of the biochar surface was determined using X-ray photoelectron spectroscopy (XPS, Escalab 250 Xi, Thermo Fisher, USA).

2.4. Adsorption experiment

Solutions contaminated with heavy metals, specifically Cd (II), Pb (II), Cr (VI), and Cr (III) were prepared using $CdCl_2$, $Pb(NO_3)_2$, $K_2Cr_2O_7$, and $CrCl_3$-$6H_2O$, respectively. These solutions were diluted with deionized water to the required concentrations for subsequent experiments. Adsorption experiments were conducted in 50 mL polyethylene centrifuge tubes. The initial concentrations of Cd (II), Pb (II), Cr (VI), and Cr (III) in the solutions were 50, 100, 50, and 50 mg/L respectively, and biochar was added at a concentration of 1g/L. Sampling was performed over a time range of 1–720 min. Adsorption kinetics experiments were conducted at 25 °C and 150 rpm to determine the optimal biochar ratio. In the adsorption isothermal experiments conducted at 25°C, the maximum adsorption capacities of FeS-CTS@nBC for Cd (II), Pb (II), Cr (VI), and Cr (III) were investigated using initial concentrations of 50–500 mg/L. Competitive ion adsorption experiments were performed to investigate the effects of different heavy metals on biochar adsorption at the same concentrations.

$$Qe = (C0 - Ce)\ V/m \quad (1)$$

The samples to be tested were filtered through a 0.22 μm filter membrane. The concentrations of Cd-(II), Pb-(II), Cr-(VI), and Cr-(III) before and after adsorption were determined by atomic absorption spectrophotometry (Z2000, Hitachi, Japan). The adsorption capacity (*Qe*) was calculated using Eq. (1), where *Qe* (mg/g) denotes the equilibrium adsorption capacity, *C0* (mg/L) denotes the initial adsorbent concentration, *Ce* (mg/L) denotes the equilibrium adsorbent concentration, *m* (g) denotes the mass of the adsorbent, and *V* (L) denotes the solution volume.

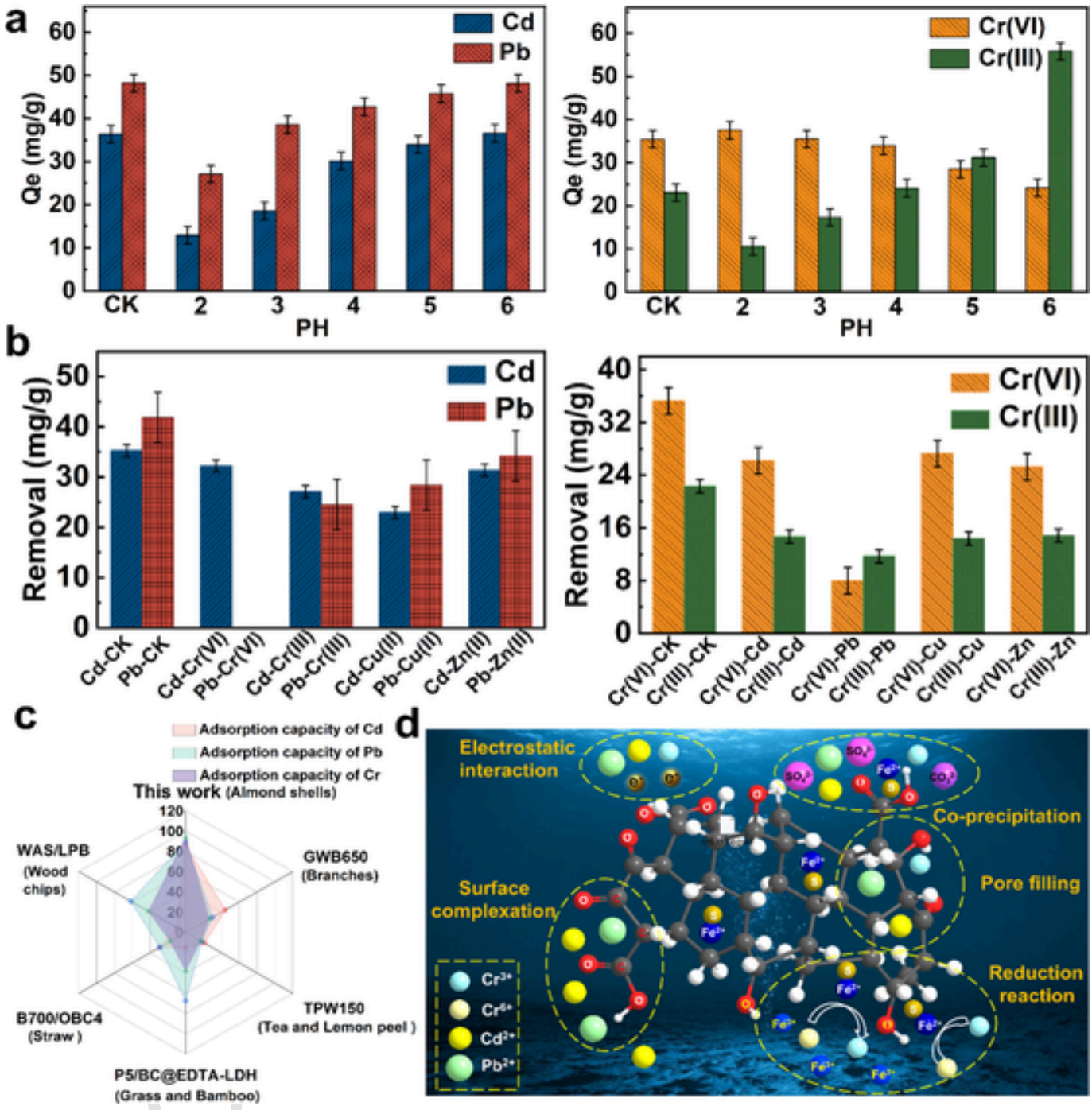

Fig. 3. The effects of different pH values on the adsorption performance of nBCS2 for Cd (II), Pb (II), Cr (VI) and Cr (III) (a); Efficiency Cd (II) removal in binary solutions containing metal cations and Cd (II) (b); The adsorption capacity comparison between this work and some biomass-based biochar (c); A schematic representation of the proposed adsorption mechanism of FeS-CTS@nBC for Cd (II), Pb (II), Cr (VI), and Cr (III) (d).

2.5. Soil remediation experiments

The soil sample (0–20 cm depth) was collected from a paddy field in Changsha City, Hunan Province, China and contaminated soil was prepared to investigate its physicochemical properties. The soil sample was air dried and passed through a 2-mm sieve. Heavy-metal contaminants were added to the test soil with $CdCl_2$, $Pb(NO_3)_2$, $K_2Cr_2O_7$, and $CrCl_3$–$6H_2O$ solutions, respectively. The contamination levels of Cd, Pb, and Cr in the single contaminated soil were maintained at 10, 100, and 150 mg kg^{-1}, respectively. The soil samples were allowed to mix well and stabilize for 2 weeks, maintaining a soil moisture content of 40 %, and were pre-incubated in an incubator at 25 ℃ [41,42]. In the 42-day remediation experiment, varying quantities of the remediation agent were added to the soil and stirred. The effects of the remediation agent on the original shape and stability of the soil were investigated. Zero (CK), 1 %, 2 %, and 3 % of the remediation agent were added to 20 g of soil. Distilled water was added to maintain the soil moisture at 50 %, and the samples were incubated at 25°C in a thermostatic incubator for 42 days. The leachability of heavy metals from nBCS2 was determined using the European Communities (BCR) continuous extraction method.

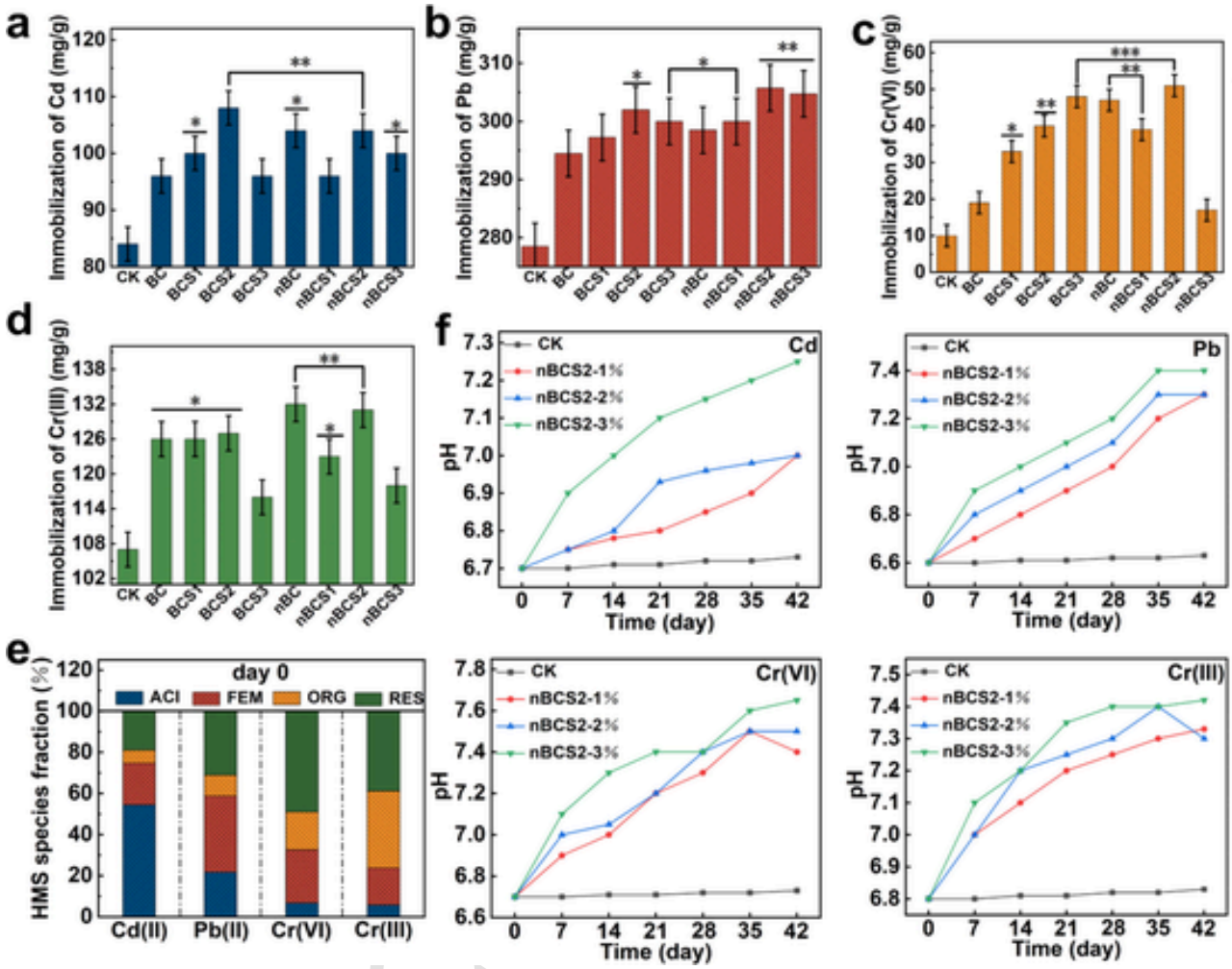

Fig. 4. The effectiveness of different biochar samples for the immobilization of heavy metals in soil (a-d); Different forms of heavy metals in soil, including acid extractable states (ACI), reducible states (FEM), oxidizable states (ORG), and residual states (RES) (e); The effect of nBCS2 biochar addition on soil pH (f). Asterisks indicate significant differences at $p < 0.05$ between the blank and experimental groups (***: $p \leq 0.001$, **: $p \leq 0.01$, *: $p \leq 0.05$).

Briefly, 1 g of each sample was extracted with 0.11 mol/L glacial acetic acid solution (pH = 2.88). The liquid–solid ratio was 40:1, and a weakly acidic extractable state was obtained by shaking the samples in a shaker at 200 rpm for 16 h at room temperature [15]. On this basis, the solid was retained after washing with deionized water. The reducible state was obtained by adding 0.5 mol/L NH_2OH–HCl and shaking for 16 h at room temperature in a shaker at 200 rpm. Ten milliliters of H_2O_2 were carefully added to the solid residue and digest in a water bath at 85°C for 1 h, reducing the solution volume to less than 3 mL. An additional 10 mL of H_2O_2 was added and the mixture was further heated until the solution volume was reduced to approximately1 mL. Subsequently, 1 mol/L NH_4OAc was added, and the mixture was shaken for 16 h at room temperature of 25 °C to obtain the oxidizable state [22]. The residual state content was determined by subtracting the amount of weak acid extraction, oxidizable, and reducible states from the total amount, which was measured using the triacid nitration method. According to the BCR continuous extraction method, the morphology of heavy metals in soil can be categorized into acidic extractive state (ACI), reduced state (FEM), oxidizable state (ORG), and residual state (RES) [25].

2.6. DFT method

The biochar model was constructed using the GaussView software, and its structure was optimized. In this study, a biochar model was constructed using several carbon rings and different oxygenated functional groups. Models of almond shell biochar were constructed both before and after modification. Before modification, the biochar contained a single and a few carbocyclic functional groups. After the modification, the number of oxygen-containing functional groups in the biochar increased. Once the structure of the biochar was optimized, a Gaussian distribution was used for the calculations. The data were imported to GaussView to plot the electrostatic potential energy and visualize the electron orbital jump of the biochar.

2.7. Pot experiment and sample collection

This study was conducted in a greenhouse at the Central South Forestry University of Science and Technology, Hunan Province, China. The experiment involved six treatments, with six replicates per treatment. Each pot contained 400 g of soil. The treatments were as follows: (1) CK; (2) contaminated soil (CS); (3) CS + 3 %BC; (4) CS + 3 %nBC; (5) CS + 3 %BCS2; and (6) CS + 3 % nBCS2. The contaminated soil had a Cd concentration of 5 ± 0.2 mg/g. For each treatment, the soil

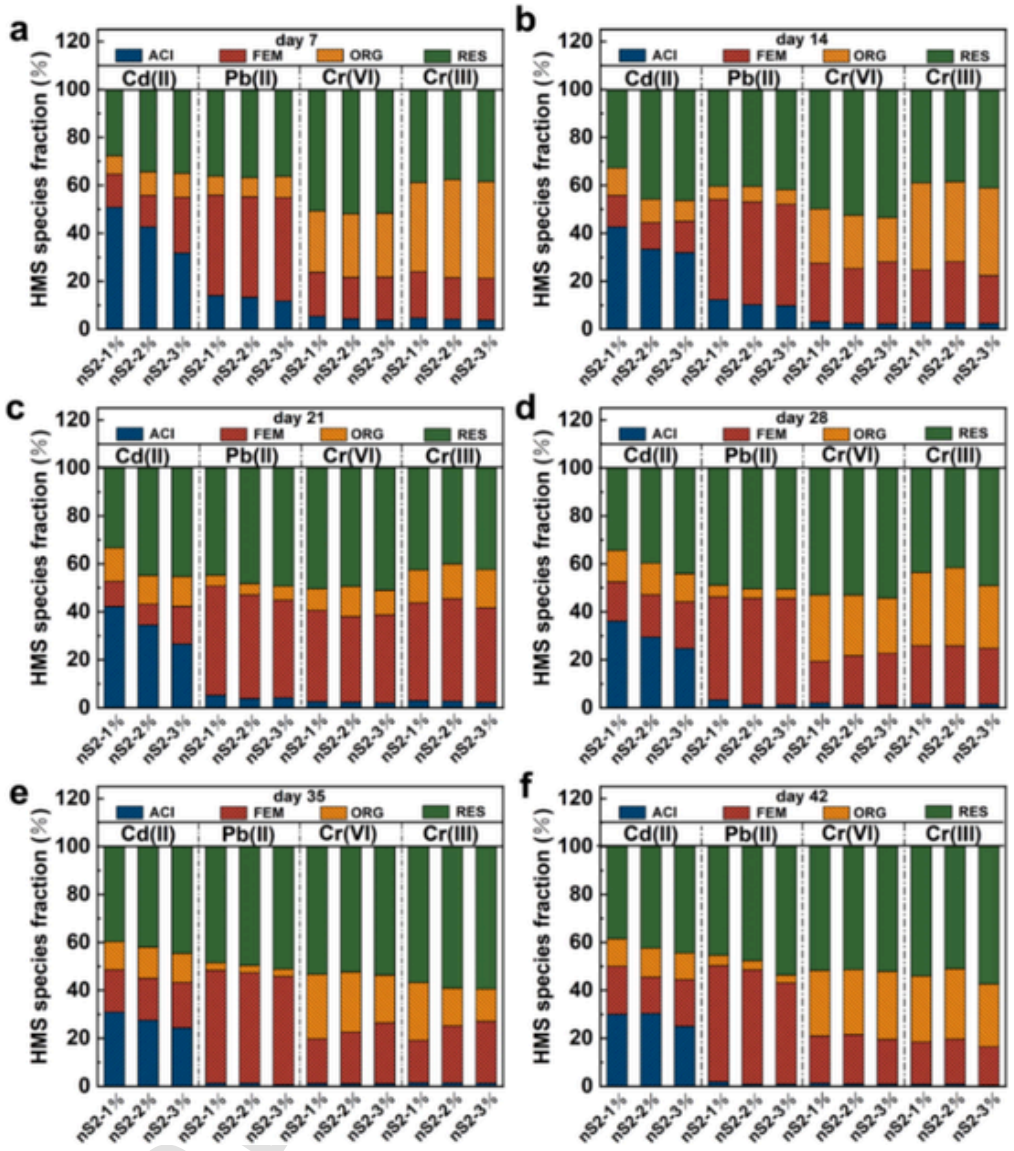

Fig. 5. The distribution of different forms of heavy metals in soil under different treatments at different time points: Day 7 (a); Day 14 (b); Day 21 (c); Day 28 (d); Day 35 (e); Day 42 (f).

was thoroughly mixed, watered, and fertilized.The paddy was fertilized once a week by adding 50 mL of the nutrient solution. The nutrient solution was prepared using 1.26 g of Hoagland's nutrient solution and 0.945 g of calcium salt, which was then heated and dissolved in 1000 mL of deionized water. After 45 days, the paddy plants were carefully removed from the soil to prevent damage to the roots and leaves, ensuring the integrity of the plant during removal. The plants were then washed and dried. Additionally, 2 cm of soil from the root zone was collected and analyzed.

3. Results and discussions

3.1. Physical and chemical properties of biochar

The surface morphology, crystalline phases and functional groups of the as-synthesized materials were characterized using SEM, XRD, XPS and FTIR. As shown in Fig. 1, the surface morphology of BC appeared smooth with a typical porous structure. Spherical FeS particles were observed in BCS2(Fig. 1b) and were, distributed within these pores. The presence of CTS helped disperse the FeS particles and prevent their excessive aggregation.

The SEM images of nBCS2 (Fig. 1c) demonstrated that after ball milling, the structure of biochar became fragmented. The larger pore size and specific surface area of nBCS2 compared to those of BC and BCS2 suggested that nBCS2 could provide more binding sites. In addition, the composition of biochar was preliminarily identified using EDS attached to the SEM. SEM-EDS was used to analyze the elemental changes in BC (Fig. 1a), BCS2 (Fig. 1b), and nBCS2 (Fig. 1c). After biochar modification, the content of Fe increased from 0 % to 6.54 %, S from 0.07 % to 3.85 %, and O from 5.90 % to 9.32 %, indicating that the modification was successful.

The functional groups, crystalline phases, and surface elements of biochar were characterized using FTIR, XRD and XPS. From the FTIR spectra (Fig. 1d), it was observed that the peaks located at 3667, 2898, 1059, and 676 cm^{-1} corresponded to O–H, C–H, C-O-C, and Fe-S, respectively. The XRD patterns of the biochar are shown in Fig. 1e. Typical carbon peaks at 19°, 22°, and 29° were observed for BC. After modification, additional peaks corresponding to FeS appeared at approxi-

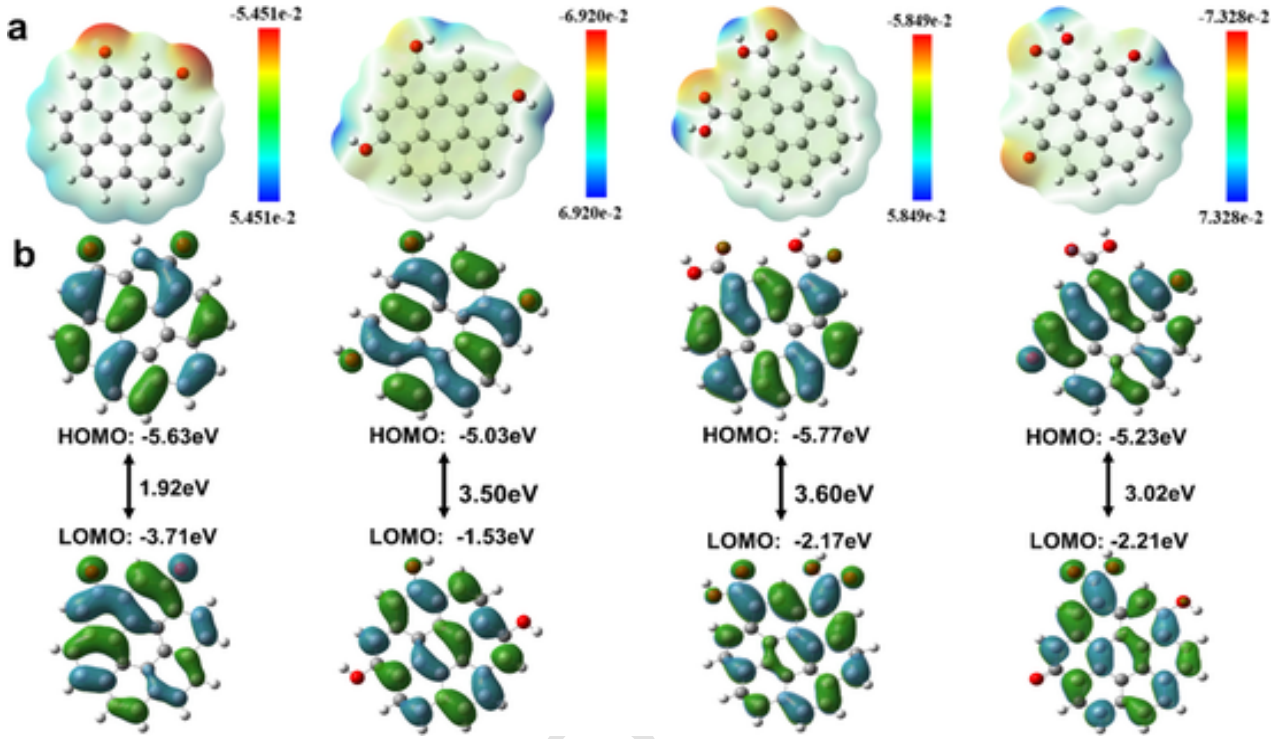

Fig. 6. All data were simulated using Gaussian software. Electrostatic potential energy (EP) on the surface of the biochar structure (a); Electronic orbital analysis of biochar enriched with –OH/–COOH groups, showing the highest occupied molecular orbital (HOMO) and the lowest unoccupied molecular orbital (LUMO) (b).

mately 14°, 23°, 27°,36, and 47°, whereas peaks corresponding to Fe_2O_3 appeared at approximately 26°,34°, and 38°. These results indicated that Fe_2O_3 and FeS were predominantly loaded onto the biochar. XPS was used to explore the functional groups on the biochar surface (Fig. 1f). The C1s spectra (Fig. 1g) showed three peaks located at 284.8, 286.0 and 289.0 eV, corresponding to C–C, C-O and C = O, respectively. The O1s with peak spectra at 533.8 eV, 532.8 eV were deconvoluted into two components: predominantly C-O–H and C-O before modification, Fe-COO and, Fe-O after the biochar was loaded with FeS. The Fe2p spectra show that the Fe (II)-S (712.1 eV, 711.5 eV) and Fe (II)-O (718.4 eV, 718.3 eV) were the predominant forms on nBCS2 (Fig. 2f) [43]. The presence of Sn^{2-} contributed to the reduction capacity of the biochar; However, Fe (II) was the key active site for the reduction of heavy metals. Additionally, S^{2-} and Sn^{2-} played a role in immobilizing heavy metals through the formation of functional groups [44].

3.2. Adsorption of biochar in water

3.2.1. Adsorption kinetics and isotherms

Kinetics and isotherms were used to evaluate the adsorption performance of FeS-CTS@nBC (Fig. 2a). Initially, the adsorption capacity increased rapidly. After a certain period, the rate of adsorption slowed and eventually reached adsorption equilibrium. When the initial solution concentration was high, there were more binding sites on the biochar facilitating fast adsorption. As the solution concentration decreased over time, the adsorption rate decreased [29,45]. The adsorption of Cd (II), Pb (II), Cr (III) by BC and nBCS2 reached equilibrium after 120 and 240 min, respectively. The adsorption equilibrium time for Cr (VI) by BC and nBCS2 was longer than the other metals. This is because the adsorption of Cd (II), Pb (II), and Cr (III) by biochar was a surface-adsorption mechanisms involving pore filling and surface complexation. However, the adsorption of Cr (VI) followed more complex and slower mechanisms, such as Fe^{2+} reduction and complexation [46].

To analyze the adsorption mechanisms and potential rate-controlling steps for the four metals, pseudo-first-order and pseudo-second-order kinetic models were applied (Fig. 2b). During the early stages of adsorption, the adsorption capacity increased exponentially. The fitted curves increased rapidly. As adsorption progressed, the rate of increase in the adsorption capacity gradually decreased and reached equilibrium after 200 min. In Fig. 2b. the horizontal coordinate represents the adsorption time and the vertical coordinate represents the adsorption capacity [18]. The adsorption of Cd (II), Pb (II), Cr (VI), and Cr (III) by BCS2 could be divided into two phases. The first stage was the rapid diffusion of ions. The amount of heavy metals adsorbed onto the BCS2 surface increased. In the second stage, heavy metals on the surface of biochar entered the interior of the biochar through intra-particle diffusion and complexed with functional groups [47,48]. Table 1 lists the fitted results for the pseudo-first-order and pseudo-second order models. The adsorption behavior of heavy metals on both types of biochar fitted well with the two kinetic models, indicating that the adsorption process involved a combination of physical and chemical adsorption [49]. For Cd (II) adsorption, nBCS2 fit better with the pseudo-first-order kinetic model, suggesting that physisorption played a major role in determining the adsorption rate. In contrast, for Pb (II), Cr (VI), and Cr (III) adsorption, both biochar composites fit the pseudo-second-order kinetic model better, indicating that the adsorption process was mainly depended on chemical interactions [50]. However, the fitting correlation between nBCS2 and pseudo-first-order kinetics was also high, which agrees with to the conclusion drawn from previous studies that nBCS2 possesses more active adsorption sites [51].

The adsorption mechanism of nBCS2 was analyzed using the Langmuir and Freundlich models (Fig. 2c). For nBCS2, within the range of 0–200 mg L^{-1}, it could adsorb almost all metal ions in the solution, with exponential increases in the adsorption amount over time. When the ion concentration was 200–500 mg L^{-1}, the adsorption capacity slowly increased and gradually reached the equilibrium. For nBCS2, the adsorption reached equilibrium at ion concentrations above 400 mg L^{-1}.

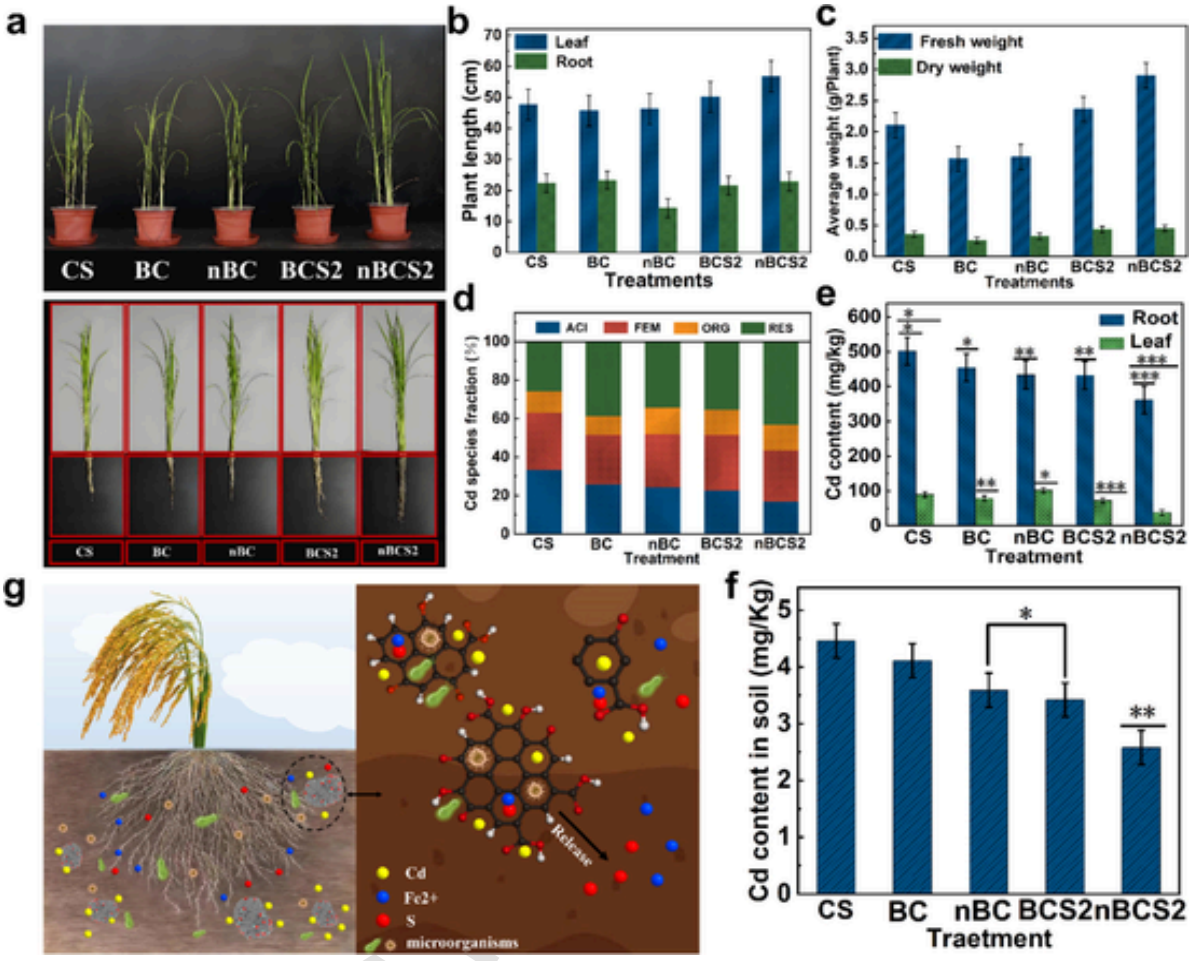

Fig. 7. Photographs of paddy growth under BC, nBC, BCS2, and nBCS2 treatments(a); Lengths of above-ground and below-ground plant parts (b); Dry and wet weights of paddy plants (c); Morphological analysis of soil heavy metals in the root system of the plant (d); In vivo heavy metal content in the plants (e); Heavy metal content in soil (f); and Schematic diagram of soil mechanism (g). Asterisks indicate significant differences at $p < 0.05$ between the blank and experimental groups (***: $p \leq 0.001$, **: $p \leq 0.01$, *: $p \leq 0.05$).

This may be because when the initial ion con-centration was low, the adsorbent could provide sufficient adsorption sites and active groups. With increasing ion concentration, the adsorption sites gradually became saturated, accompanied by a decrease in active sites and saturation of the adsorbent [35]. The FeS-CTS modification enhanced the functional groups (e.g., –OH and –COOH) and metal binding sites (e.g., Fe-O and Fe-S) on the biochar, whereas the adsorption performance of nBCS2 was enhanced after ball milling. The adsorption data were evaluated using Langmuir and Freundlich models (Table S2). The Langmuir and Freundlich models are suitable for describing monolayer and multilayer adsorption, respectively. The adsorption of Cd (II), Pb (II), Cr (VI) and Cr (III) by biochar was deemed a complex mechanism, involving monolayer adsorption (pore filling and surface complexation) and multilayer adsorption (diffusion of heavy metal ions within the pores). The use of both the Langmuir and Freundlich models helped improve the accuracy and practicality of describing adsorption process [52]. Adsorption is a complex process in which the adsorbent has a limited number of adsorption sites and finite adsorption capacity, eventually reaching adsorption equilibrium over time. Furthermore, the adsorption sites are not fixed, and the adsorbent can adsorb a variety of substances. Therefore, the Langmuir and Freundlich models were selected for adsorption isotherm fitting [53]. These results indicated that the adsorption of Cd (II) and, Cr (VI) by biochar followed a homogeneous monolayer adsorption process, whereas the adsorption of Pb (II) and, Cr (III) followed heterogeneous multilayer adsorption [49,54]. The 1/n value < 1 for the Freundlich model indicated that the adsorption of metals by nBCS2 was a favorable process [55,56].

3.2.2. *Effect of solution pH and competitive adsorption*

The effect of the pH on the adsorption of heavy metals was also investigated (Fig. 3a). As the pH increased from 2 to 6, the adsorption of nBCS2 for Cd (II), Pb (II), and Cr (III) increased dramatically, whereas that the adsorption of Cr (VI) decreased. At a low pH, the hydroxyl functional groups on the nBCS2 surface were easily protonated. Many H^+ ions competed with metal cations and caused electrostatic repulsion, which reduced the binding of metal ions to acidic functional groups [57]. As the pH increased, the electrostatic repulsion decreased. The negative charge on the biochar surface increased and the positive charge decreased, which was favorable for the immobilization of Cd (II), Pb (II), and Cr (III). A high pH accelerated the formation of cationic oxides and hydroxides such as Cd (II), Pb (II), and Cr (III). In general, the reduction of Cr (VI) is more favorable in acidic environments, where Cr (VI) reacts with acids to form insoluble precipitates [38,58]. It was observed that, is the pH increased, and the concentration of H^+ decreased, the removal of Cr (VI) by nBCS2 was affected.

Many types of heavy metals are present in wastewater. Therefore, understanding the competitive behavior of co-existing cations and adsorption selectivity is important for the practical application of biochar.

As shown in Fig. 3b, Cr (VI) and Zn (II) clearly inhibited Cd (II) adsorption. In contrast, the presence of Cr (III) and Cu (II) did not significantly affect Cd (II) adsorption. The decreased Cd (II) removal was attributed to the competition between cations for active sites, resulting in decreased adsorption [59,60]. In the Cr (VI)- Pb (II) system, Pb (II) was not detected because of the following reaction:

$$2Pb(NO_3)_2 + K_2Cr_2O_7 + H_2O = 2PbCrO_4\downarrow + 2KNO_3 + 2HNO_3$$

In addition, electronegativity was deemed an important factor in determining the strength of competitive adsorption between metal cations and nBCS2. The electronegativities of Pb, Cu, Zn, Cr, and Cd were 2.33, 1.90, 1.65, 1.66, and 1.69, respectively [61]. Cations with higher electronegativity were more likely to form chemical bonds with nBCS2. The adsorption capacity of FeS-CTS@nBC was compared with that of previously reported biomass-based biochar such as wood chips, bamboo, lemon peel, and rice straw, and the results are shown in Fig. 3c. The adsorption capacity of FeS-CTS@nBC was superior to that of some biomass-based biochar [62–69].

The mechanism of heavy-metal removal by FeS-CTS@nBC is illustrated in Fig. 3d. The modification of CTS increased the oxygenated functional groups of the biochar and enhanced its heavy-metal removal capacity. The removal mechanism for Cr (VI) was that Fe^{2+} reduced Cr (VI) to Cr (III) and Fe^{2+} was subsequently oxidized to Fe^{3+} [70]. Overall, we conclude that electrostatic interactions, complexation, co-precipitation, ferrous reduction, and pore filling are the main adsorption mechanisms of FeS-CTS@nBC. The reactive groups of biochar, such as carboxyl, sulfhydryl, hydroxyl, and amino groups, interacted with heavy metals to form insoluble complexes. Large amounts of CO_3^{2-} and SO_4^{2-} in water co-precipitated with heavy metals in the sediment [71, 72]. The physical adsorption capacity of FeS-CTS@nBC was enhanced by ball milling, and pore filling played a role in the immobilization of heavy metals. Secondary effects, such as ion exchange also played a role in the immobilization of heavy metals.

3.3. Adsorption of biochar in soil

Soil fixation experiments were performed to analyze the effects of biochar on the immobilization of heavy metals in the soil. As shown in Fig. 4a, the blank group (CK) contained only soil. Compared to the CK, the experimental group treated with biochar showed an increase in the immobilization of heavy metals. Overall, nBCS2 had a stronger better effect on the immobilization of heavy metals. The morphology of heavy metals in the contaminated soil was investigated using the BCR continuous extraction method (Fig. 4e). The effect of biochar addition on the soil pH was also investigated (Fig. 4f). FeS-CTS@nBC was alkaline and the initial pH of the soil was weakly acidic. The soil pH increased after biochar addition. Fig. 4f shows the change in soil pH after 42 days of nBCS2 addition. The original soil pH values of Cd (II), Pb (II), Cr (VI) and Cr (III) ranged from 6.6 to 6.8. The addition of nBCS2 increased soil pH. Therefore, when applying nBCS2, its pH should be adjusted according to the pH of the soil. nBCS2, with a high alkaline ratio suitable for the remediation of acidic soil.

The BCR continuous extraction method was used to further evaluate the various forms of heavy metals in the soil before and after FeS-CTS@nBC remediation (Fig. 5). As stated earlier, heavy metals in soil can be divided into different states: ACI, FEM, ORG, and RES. ACI could migrate with soil moisture and affect soil ecology. The contents of ORG and FEM changed with changes in soil pH, whereas RES did not migrate. The ACI of Cd, Pb, Cr (VI), and Cr (III) in the CK group were 54.43 %, 24.81 %, 6.63 %, and 5.71 %, respectively (Fig. 5a). After 42 days of treatment, the ACI of Cd, Pb, Cr (VI), and Cr (III) in the soil decreased to 29.43 %, 23.93 %, 5.75 %, and 5.23 % respectively, with the 3 % nBCS2 treatment (Fig. 5f). As more nBCS2 was added, the percentages of ACI decreased. In this work, the RES of heavy metals increased, whereas the ACI decreased, with the addition of biochar. The term "reducible fraction" described the portion of heavy metals that could be broken down by plants and soil. The ORG and FEM of the heavy metals exhibited morphological stability and were more difficult to leach from the soil. The fixation and stabilization of heavy metals were enhanced by FeS-CTS@nBC by promoting the conversion of ACI and FEM into ORG and RES components. In addition, microbial growth can help reduce heavy metals in soil [35].

3.4. DFT calculations

Based on the DFT calculations, the micro-mechanisms at the electron-scale for the adsorption of Cd (II), Pb (II), Cr (VI), and Cr (III) on biochar were investigated. The electrostatic potential energy (EP) reflects the ability of biochar to accept and transfer electrons. It was easy to transfer electrons under low-EP conditions, with the red part indicating a negative EP, in which it was easy to deliver electrons [73]. As shown in Fig. 6a, when modified with C═O/–OH /–COOH groups, the EP values in the vicinity of oxygen atoms of these groups were negative [40]. These results indicate that macromolecules with low EP interact more easily with heavy metals. Therefore, oxygen atoms with a lower EP were found to be more prone to interacting with heavy metals, explaining why oxygen-containing functional groups were more likely to immobilize heavy metals.

Chemical adsorption of heavy metals by biochar can be viewed as the transition of electrons from the highest occupied molecular orbital (HOMO) to the lowest unoccupied molecular orbital (LUMO). A larger energy gap (Eg) between the HOMO and LUMO of biochar indicates greater potential for spontaneous electron mobility and stronger adsorption capacity for heavy metals [63]. As shown in Fig. 6b, biochar enriched with –OH and –COOH had the largest energy gap and the strongest adsorption capacity. The results showed that the adsorption performance of FeS-CTS@nBC was stronger and that the oxygen-containing functional groups were superior in the immobilization of heavy metals [59,74]. The positive and negative values of the phases are represented in blue and green in Fig. 6b. For the –OH and –COOH enriched biochar samples, the electron distribution of the HOMO was concentrated, indicating a considerably greater electron donating capacity in this region and the removal of heavy metals. Additionally, the HOMO and LUMO values of the adsorbent can be used to visually predict the optimal absorption sites in the adsorption process.

3.5. Effect of remediated soil on rice growth

The observation of plant growth in contaminated soil after biochar remediation could be an indicator of the effectiveness of biochar. Fig. 7 shows the growth status of the paddies under different treatments. As shown in Fig. 7a, compared with the original Cd-contaminated soil, paddies grown in soil restored with nBCS2 showed better growth. The leaves and roots of the paddy were slender and dense, respectively. The restorative effect of nBCS2 most directly reflected the length and weight of the paddy plants. As shown in Fig. 7b, the leaf and root lengths of the paddy in the original Cd-polluted soil were only 47.25 and 21.4 cm, respectively. The leaf and root lengths of the paddy in the nBCS2 repaired soil were 56.84 and 25.83 cm, respectively. The total length of the paddy fields was 19.98 % greater than that of the Cd-contaminated soil. According to the average dry and wet weight data of the paddy shown in Fig. 7c, the dry and wet weights of the CS-treated soil were 0.223 and 1.13 g/plant, respectively. In contrast, the dry and wet weights of paddy fields grown in the nBCS2-restored soil were 0.452 and 2.903 g/plant, respectively. These results demonstrate that nBCS2 significantly promoted the growth of paddy fields, as indicated by increased plant length and biomass. The enhanced growth can be attributed to the presence of Fe^{2+} and S^{2-} in the modified biochar, which stimulated paddy development.

To investigate the effect of modified biochar on heavy metals in the soil, the heavy metal contents of paddy and rhizosphere soils were analyzed [75,76]. From Fig. 7d, it could be seen that the migration of Cd from the amended soil to paddy was significantly reduced, particularly in the CS + nBCS2 group, where the Cd content in the paddy roots and leaves was the lowest. Compared with the CS group, the ACI of Cd in the soil was significantly reduced and the RES increased after the addition of biochar. The ACI of Cd in the soil was lowest in the nBCS2 treatment. As shown in Fig. 7e, the Cd content of CS-treated paddy was 591.62 mg/kg, with 501.73 mg/kg in the roots and 89.89 mg/kg in the leaves. In the paddy grown in the soil restored with nBCS2, the Cd content decreased by 32.47 %, and the Cd concentrations in the roots and leaves decreased by 27.91 % and 57.95 %, respectively. The soil remediated with nBCS2 had the lowest volume of heavy metals in Fig. 7f. After soil remediation, part of Cd was immobilized in the FeS-CTS modified almond shell biochar, making it difficult for it migrate to the plants, thereby reducing the toxic effects of Cd on the paddy.

4. Conclusions

In this study, almond shell biochar was prepared by pyrolysis and modified with FeS-CTS. The performance of FeS-CTS@nBC in the adsorption of heavy metals was investigated. Compared to the unmodified almond shell biochar, FeS-CTS@nBC exhibited a higher adsorption performance for heavy metals. Organic matter and element enriched FeS-CTS@nBC effectively improved the soil nutrient contents and promoted paddy growth. After 42 days of incubation, the steady state of Cd in the 3 % nBCS2-treated soil increased, which was more favorable for paddy growth and inhibited the migration of heavy metals into the seedlings, leading to a significant decrease in the bioaccumulation of Cd in both the roots and leaves. Overall, FeS-CTS@nBC is an efficient adsorbent for the removal of heavy metals and has great potential for applications in the adsorption of heavy metals.

CRediT authorship contribution statement

Penghui Guo: Formal analysis, Methodology, Writing – review & editing. **Xiang Gu:** Validation. **Zhaoshuang Li:** Project administration, Funding acquisition. **Xu Xu:** Data curation. **Yini Cao:** Conceptualization, Project administration. **Guoen Yang:** Investigation. **Chuntao Kuang:** Investigation. **Xingong Li:** Data curation. **Yan Qing:** Data curation. **Yiqiang Wu:** Methodology, Project administration.

Declaration of competing interest

The authors declare that they have no known competing financial interests or personal relationships that could have appeared to influence the work reported in this paper.

Data availability

Data will be made available on request.

Appendix A. Supplementary data

Supplementary data to this article can be found online at https://doi.org/10.1016/j.seppur.2024.130943.

References

[1] J. Zhu, Y. Song, L. Wang, Z. Zhang, J. Gao, D.C.W. Tsang, Y.S. Ok, D. Hou, Green remediation of benzene contaminated groundwater using persulfate activated by biochar composite loaded with iron sulfide minerals, Chem. Eng. J. 429 (2022).

[2] M. Zhang, G. Song, D.L. Gelardi, L. Huang, E. Khan, O. Mašek, S.J. Parikh, Y.S. Ok, Evaluating biochar and its modifications for the removal of ammonium, nitrate, and phosphate in water, Water Res. 186 (2020).

[3] J. Yuan, C. Wan, S. Wei, H. Chai, T. Tao, Research progress on the application of nanocellulose in glucose sensing, Curr. Org. Synth. 21 (2024).

[4] D. Wu, Y. Wang, Y. Li, Q. Wei, L. Hu, T. Yan, R. Feng, L. Yan, B. Du, Phosphorylated chitosan/CoFe2O4 composite for the efficient removal of Pb (II) and Cd (II) from aqueous solution: adsorption performance and mechanism studies, J. Mol. Liq. 277 (2019) 181–188.

[5] H. Wang, R. Liu, Q. Chen, H. Xia, Y. Zhang, Novel Chitosan-FeS@biochar-added constructed wetland microcosms for NH^{4+}/NO_3^- and Pb removal: Performance and mechanism, J. Environ. Chem. Eng. 11 (2023).

[6] P. Staroń, A. Zawadzka, P. Radomski, J. Chwastowski, Characteristics of removal of lead, cadmium and chromium from soil using biosorbent and biochar, Appl. Sci. 14 (2024).

[7] A. Herath, C.A. Layne, F. Perez, E.I.B. Hassan, C.U. Pittman, T.E. Mlsna, KOH-activated high surface area Douglas Fir biochar for adsorbing aqueous Cr (VI), Pb (II) and Cd (II), Chemosphere 269 (2021).

[8] B. Wang, B. Gao, Y. Wan, Entrapment of ball-milled biochar in Ca-alginate beads for the removal of aqueous Cd(II), J. Ind. Eng. Chem. 61 (2018) 161–168.

[9] M. Turk Sekulić, S. Pap, Z. Stojanović, N. Bošković, J. Radonić, T. Šolević Knudsen, Efficient removal of priority, hazardous priority and emerging pollutants with Prunus armeniaca functionalized biochar from aqueous wastes: Experimental optimization and modeling, Sci. Total Environ. 613–614 (2018) 736–750.

[10] N. Seyedi, M. Ahmadyousefi, N.S. Marghaki, R. Afsharipour, M. Jahanshahi, M.A. Nezhad, High-efficiency adsorption of heavy metals on sulfur nanoparticles coated biochar derived from alfalfa residues and its biological effects, Biomass Convers. Biorefin. (2023).

[11] L. Qian, H. Li, Z. Wei, C. Liang, X. Dong, D. Lin, M. Chen, Enhanced removal of cis-1,2-dichloroethene and vinyl chloride in groundwater using ball-milled sulfur- and biochar-modified zero-valent iron: From the laboratory to the field, Environ. Pollut. 336 (2023).

[12] S. Mandal, S. Pu, L. Shangguan, S. Liu, H. Ma, S. Adhikari, D. Hou, Synergistic construction of green tea biochar supported nZVI for immobilization of lead in soil: A mechanistic investigation, Environ. Int. 135 (2020).

[13] T. Liu, Y. Zhou, W. Zheng, C. Chang, J. Dong, J. Wen, X. Zheng, FeS/MgO-biochar composites for boosting the adsorption-photocatalytic degradation of RhB, Mater. Sci. Semicond. Process. 174 (2024).

[14] H. Lyu, S. Xia, J. Tang, Y. Zhang, B. Gao, B. Shen, Thiol-modified biochar synthesized by a facile ball-milling method for enhanced sorption of inorganic Hg^{2+} and organic $CH3Hg^+$, J. Hazard. Mater. 384 (2020).

[15] X. Liu, D. Li, J. Li, J. Wang, S. Liang, H. Deng, A novel MnOx-impregnated on peanut shells derived biochar for high adsorption performance of Pb (II) and Cd (II): Behavior and mechanism, Surf. Interfaces 34 (2022).

[16] S. Yu, J. He, Z. Zhang, Z. Sun, M. Xie, Y. Xu, X. Bie, Q. Li, Y. Zhang, M. Sevilla, M.M. Titirici, H. Zhou, Towards negative emissions: hydrothermal carbonization of biomass for sustainable carbon materials, Adv. Mater. 36 (2024).

[17] J. Yu, H. Feng, L. Tang, Y. Pang, J. Wang, J. Zou, Q. Xie, Y. Liu, C. Feng, J. Wang, Insight into the key factors in fast adsorption of organic pollutants by hierarchical porous biochar, J. Hazard. Mater. 403 (2021).

[18] J. Jiang, R. Li, K. Yang, Y. Li, L. Deng, D. Che, Investigation on Pb^{2+} adsorption characteristics by AAEMs-rich biochar in aqueous solution: Performance and mechanism, Environ. Res. 236 (2023).

[19] V.Y. Ko, J. Wang, I. He, D. Ryan, X. Zhang, C. Lan, Adsorption of methane on biochar for emission reduction in oil and gas fields, Biochar 5 (2023).

[20] A. Liang, C. Ma, J. Xiao, Y. Hao, H. Li, Y. Guo, Y. Cao, W. Jia, L. Han, G. Chen, Q. Tan, J.C. White, B. Xing, Micro/nanoscale bone char alleviates cadmium toxicity and boosts rice growth via positively altering the rhizosphere and endophytic microbial community, J. Hazard. Mater. 454 (2023).

[21] A. Li, Y. Zhang, W. Ge, Y. Zhang, L. Liu, G. Qiu, Removal of heavy metals from wastewaters with biochar pyrolyzed from MgAl-layered double hydroxide-coated rice husk: mechanism and application, Bioresour. Technol. 347 (2022).

[22] S. Fan, Y. Wang, Z. Wang, J. Tang, J. Tang, X. Li, Removal of methylene blue from aqueous solution by sewage sludge-derived biochar: adsorption kinetics, equilibrium, thermodynamics and mechanism, J. Environ. Chem. Eng. 5 (2017) 601–611.

[23] X. Li, S. Zhang, J.-J. Tang, J. Yang, K. Wen, J. Wang, P. Wang, X.-Y. Zhou, Y.-G. Zhang, Structural design of biomass-derived hard carbon anode materials for superior sodium storage via increasing crystalline cellulose and closing the open pores, J. Mater. Chem. A 12 (2024) 21176–21189.

[24] X. Jin, R. Liu, H. Wang, L. Han, M. Qiu, B. Hu, Functionalized porous nanoscale Fe3O4 particles supported biochar from peanut shell for Pb(II) ions removal from landscape wastewater, Environ. Sci. Pollut. Res. 29 (2022) 37159–37169.

[25] X.-Z. Fu, J. Wu, S. Cui, X.-M. Wang, H.-Q. Liu, R.-L. He, C. Yang, X. Deng, Z.-L. Tan, W.-W. Li, Self-regenerable bio-hybrid with biogenic ferrous sulfide nanoparticles for treating high-concentration chromium-containing wastewater, Water Res. 206 (2021).

[26] J. Fan, X. Chen, Z. Xu, X. Xu, L. Zhao, H. Qiu, X. Cao, One-pot synthesis of nZVI-embedded biochar for remediation of two mining arsenic-contaminated soils: Arsenic immobilization associated with iron transformation, J. Hazard. Mater. 398 (2020).

[27] J. Fan, C. Cai, H. Chi, B.J. Reid, F. Coulon, Y. Zhang, Y. Hou, Remediation of cadmium and lead polluted soil using thiol-modified biochar, J. Hazard. Mater. 388 (2020).

[28] Z. Jin, Z. Xue, B. Li, L. Ou, L. Yan, L. Yang, K. Yin, J. Jouha, P. Shao, Z. Zeng, S. Luo, High-performance spent coffee grounds-based 3D microporous biochar for the efficient capture of Cd2+ via a multi-pathway mechanism, Chem. Eng. J. 485 (2024).

[29] M. Yin, X. Bai, D. Wu, F. Li, K. Jiang, N. Ma, Z. Chen, X. Zhang, L. Fang, Sulfur-

functional group tunning on biochar through sodium thiosulfate modified molten salt process for efficient heavy metal adsorption, Chem. Eng. J. 433 (2022).
[30] C. Chen, M. Qiu, High efficiency removal of Pb (II) in aqueous solution by a biochar-supported nanoscale ferrous sulfide composite, RSC Adv. 11 (2021) 953–959.
[31] A. Alcazar-Ruiz, A. Villardon, F. Dorado, L. Sanchez- Silva, Hydrothermal carbonization coupled with fast pyrolysis of almond shells: valorization and production of valuable chemicals, Waste Manag. 169 (2023) 112–124.
[32] A. Li, W. Ge, L. Liu, Y. Zhang, G. Qiu, Synthesis and application of amine-functionalized MgFe2O4-biochar for the adsorption and immobilization of Cd (II) and Pb (II), Chem. Eng. J. 439 (2022).
[33] G. Zhou, F. Gao, T. Liu, S. Shi, H. Wang, Y. Yuan, N. Wang, Polyamidoxime-coated coconut haustorium derived magnetic biochar adsorbent with photothermal conversion for highly efficient uranium recovery from nuclear wastewater, Adv. Funct. Mater. (2024).
[34] S. Batool, M. Idrees, M.I. Al-Wabel, M. Ahmad, K. Hina, H. Ullah, L. Cui, Q. Hussain, Sorption of Cr(III) from aqueous media via naturally functionalized microporous biochar: Mechanistic study, Microchem. J. 144 (2019) 242–253.
[35] L. Tan, Y. Nie, H. Chang, L. Zhu, K. Guo, X. Ran, N. Zhong, D. Zhong, Y. Xu, S.-H. Ho, Adsorption performance of Ni(II) by KOH-modified biochar derived from different microalgae species, Bioresour. Technol. 394 (2024).
[36] F. Du, L. Liu, Y. Pan, C. Wu, R. Wang, Z. Zhao, W. Fan, H. Song, Y. Shi, J. Wang, A novel biochar-based composite hydrogel for removing heavy metals in water and alleviating cadmium stress in tobacco seedlings, Sci. Rep. 13 (2023).
[37] F. Huang, F. Dong, L. Chen, Y. Zeng, L. Zhou, S. Sun, Z. Wang, J. Lai, L. Fang, Biochar-mediated remediation of uranium-contaminated soils: evidence, mechanisms, and perspectives, Biochar 6 (2024).
[38] T.-T. Qian, P. Wu, Q.-Y. Qin, Y.-N. Huang, Y.-J. Wang, D.-M. Zhou, Screening of wheat straw biochars for the remediation of soils polluted with Zn (II) and Cd (II), J. Hazard. Mater. 362 (2019) 311–317.
[39] X. Su, X. Wang, Z. Ge, Z. Bao, L. Lin, Y. Chen, W. Dai, Y. Sun, H. Yuan, W. Yang, J. Meng, H. Wang, S.C. Pillai, KOH-activated biochar and chitosan composites for efficient adsorption of industrial dye pollutants, Chem. Eng. J. 486 (2024).
[40] Y. Sun, C. Liu, Y. Gao, T. Zhang, Y. Jia, S. Wang, All-in-one strategy to prepare molded biochar with magnetism from sewage sludge for high-efficiency removal of Cd(II), J. Hazard. Mater. 454 (2023).
[41] Y. Wang, X. Wang, Z. Bing, Q. Zhao, K. Wang, J. Jiang, M. Jiang, Q. Wang, R. Xue, Remediation of Cd(II), Zn(II) and Pb(II) in contaminated soil by KMnO4 modified biochar: Stabilization efficiency and effects of freeze–thaw ageing, Chem. Eng. J. 487 (2024).
[42] Q. Liu, C. Wu, L. Wei, S. Wang, Y. Deng, W. Ling, W. Xiang, Y. Kuzyakov, Z. Zhu, T. Ge, Microbial mechanisms of organic matter mineralization induced by straw in biochar-amended paddy soil, Biochar 6 (2024).
[43] Z. Li, Y. Huang, Z. Zhu, M. Yu, H. Cheng, H. Shi, Y. Xiao, H. Song, W. Zuo, H. Zhou, S. Wang, Attempts to obtain clean biochar from hyperaccumulator through pyrolysis: Removal of heavy metals and transformation of phosphorus, J. Hazard. Mater. 468 (2024).
[44] Y. Wan, H. Luo, Y. Cai, Z. Dang, H. Yin, Selective removal of total Cr from a complex water matrix by chitosan and biochar modified-FeS: Kinetics and underlying mechanisms, J. Hazard. Mater. 454 (2023).
[45] W. Zhang, Y. Cho, M. Vithanage, S.M. Shaheen, J. Rinklebe, D.S. Alessi, C.-H. Hou, Y. Hashimoto, P.A. Withana, Y.S. Ok, Arsenic removal from water and soils using pristine and modified biochars, Biochar 4 (2022).
[46] S. Wang, S. Guo, Effects of soil organic carbon metabolism on electro-bioremediation of petroleum-contaminated soil, J. Hazard. Mater. 459 (2023).
[47] Z. Liu, Z. Li, S. Chen, W. Zhou, Enhanced phytoremediation of petroleum-contaminated soil by biochar and urea, J. Hazard. Mater. 453 (2023).
[48] J. Liu, S. Jiang, D. Chen, G. Dai, D. Wei, Y. Shu, Activation of persulfate with biochar for degradation of bisphenol A in soil, Chem. Eng. J. 381 (2020).
[49] A.A. Abdelhafez, J. Li, M.H.H. Abbas, Feasibility of biochar manufactured from organic wastes on the stabilization of heavy metals in a metal smelter contaminated soil, Chemosphere 117 (2014) 66–71.
[50] Y. Cheng, A. Li, W. Shi, L. Zhao, Magnetic chitosan-functionalized waste carton biochar composites for efficient adsorption of anionic and cationic dyes, Chem. Eng. J. 481 (2024).
[51] Z.-H. Bian, M. Wang, J.-H. Huang, R. Liang, J.-D. Du, C.-C. Fang, C. Shen, Y.-B. Man, M.-H. Wong, S.-G. Shan, J. Zhang, Large particle size boosting the engineering application potential of functional biochar in ammonia nitrogen and phosphorus removal from biogas slurry, J. Water Process Eng. 57 (2024).
[52] X. Shang, S. Wu, Y. Liu, K. Zhang, M. Guo, Y. Zhou, J. Zhu, X. Li, R. Miao, Rice husk and its derived biochar assist phytoremediation of heavy metals and PAHs co-contaminated soils but differently affect bacterial community, J. Hazard. Mater. 466 (2024).
[53] Lu. Lei, C. Na, Gibbsian interpretation of Langmuir, Freundlich and Temkin isotherms for adsorption in solution, Philos. Mag. Lett. 102 (2022) 239–253.
[54] F.U. Haider, N.-U. Ain, I. Khan, M. Farooq, L. Habiba, Y.L. Cai, Co-application of biochar and plant growth regulators improves maize growth and decreases Cd accumulation in cadmium-contaminated soil, J. Clean. Prod. 440 (2024).
[55] D. Vamvuka, K. Stergiou, E. Sdoukou, A. Stratakis, Magnesium or bentonite modified almond kernel biochar for phosphate adsorption from contaminated water solutions, J. Environ. Chem. Eng. 12 (2024).
[56] Z.-H. Yang, S. Xiong, B. Wang, Q. Li, W.-C. Yang, Cr (III) adsorption by sugarcane pulp residue and biochar, J. Cent. South Univ. 20 (2013) 1319–1325.
[57] L.R. Ortiz, E. Torres, D. Zalazar, H. Zhang, R. Rodriguez, G. Mazza, Influence of pyrolysis temperature and bio-waste composition on biochar characteristics, Renew. Energy 155 (2020) 837–847.
[58] H. Wang, Z. Tian, L. Jiang, W. Luo, Z. Wei, S. Li, J. Cui, W. Wei, Highly efficient adsorption of Cr(VI) from aqueous solution by Fe^{3+} impregnated biochar, J. Dispers. Sci. Technol. 38 (2016) 815–825.
[59] C. Ren, X. Ding, W. Li, H. Wu, H. Yang, Highly efficient adsorption of heavy metals onto novel magnetic porous composites modified with amino groups, J. Chem. Eng. Data 62 (2017) 1865–1875.
[60] M. Maslova, V. Ivanenko, N. Yanicheva, L. Gerasimova, The effect of heavy metal ions hydration on their sorption by a mesoporous titanium phosphate ion-exchanger, J. Water Process Eng. 35 (2020).
[61] H.M. El Mashad, A. Edalati, R. Zhang, B.M. Jenkins, Production and characterization of biochar from almond shells, Clean Technol. 4 (2022) 854–864.
[62] Z. Aslam, M. Khalid, M. Naveed, M. Shahid, M. Aon, Evaluation of green waste and popular twigs biochar produced at low and high pyrolytic temperature for efficient removal of metals from water, Water Air Soil Pollut. 228 (2017).
[63] T. Chi, J. Zuo, F. Liu, Performance and mechanism for cadmium and lead adsorption from water and soil by corn straw biochar, Front. Environ. Sci. Eng. 11 (2017).
[64] C. Zhang, B. Shan, W. Tang, Y. Zhu, Comparison of cadmium and lead sorption by Phyllostachys pubescens biochar produced under a low-oxygen pyrolysis atmosphere, Bioresour. Technol. 238 (2017) 352–360.
[65] B. Birgili, H. Haykiri-Acma, S. Yaman, Biosorption of lead, hexavalent chrome and cadmium from aqueous solution by torrefied biomass, Int. J. Environ. Sci. Technol. 21 (2024) 8049–8062.
[66] S. Cairns, S. Chaudhuri, G. Sigmund, I. Robertson, N. Hawkins, T. Dunlop, T. Hofmann, Wood ash amended biochar for the removal of lead, copper, zinc and cadmium from aqueous solution, Environ. Technol. Innov. 24 (2021).
[67] D. Huang, C. Liu, C. Zhang, R. Deng, R. Wang, W. Xue, H. Luo, G. Zeng, Q. Zhang, X. Guo, Cr (VI) removal from aqueous solution using biochar modified with Mg/Al-layered double hydroxide intercalated with ethylenediaminetetraacetic acid, Bioresour. Technol. 276 (2019) 127–132.
[68] A. Ahmadian, B.A. Goharrizi, T. Shahriari, S. Ahmadi, Adsorption of chromium (VI) and Acid Orange 7 on lemon peel biochar: a response surface methodology approach, Int. J. Environ. Sci. Technol. 20 (2022) 2939–2958.
[69] A. Dahiya, A. Bhardwaj, A. Rani, M. Arora, J.N. Babu, Reduced and oxidized rice straw biochar for hexavalent chromium adsorption: Revisiting the mechanism of adsorption, Heliyon 9 (2023).
[70] Y. Liu, L. Wang, X. Wang, F. Jing, R. Chang, J. Chen, Oxidative ageing of biochar and hydrochar alleviating competitive sorption of Cd (II) and Cu (II), Sci. Total Environ. 725 (2020).
[71] S. Tang, J. Gong, B. Song, W. Cao, J. Li, Remediation of biochar-supported effective microorganisms and microplastics on multiple forms of heavy metals in eutrophic lake, J. Hazard. Mater. 465 (2024).
[72] B. Liu, T. Chen, B. Wang, S. Zhou, Z. Zhang, Y. Li, X. Pan, N. Wang, Enhanced removal of Cd2 + from water by AHP-pretreated biochar: Adsorption performance and mechanism, J. Hazard. Mater. 438 (2022).
[73] X. Li, R. Li, M. Zhan, Q. Hou, H. Zhang, G. Wu, L. Ding, X. Lv, Y. Xu, Combined magnetic biochar and ryegrass enhanced the remediation effect of soils contaminated with multiple heavy metals, Environ. Int. 185 (2024).
[74] P. Wang, M. Yu, P. Lin, Y. Zheng, L. Ren, Effects of biochar supported nano zero-valent iron with different carbon/iron ratios on two-phase anaerobic digestion of food waste, Bioresour Technol 382 (2023).
[75] W. Chi, Q. Nan, Y. Liu, D. Dong, Y. Qin, S. Li, W. Wu, Stress resistance enhancing with biochar application and promotion on crop growth, Biochar 6 (2024).
[76] H. Zhang, H. Yang, J. Shao, Y. Chen, S. Zhang, H. Chen, Multifunctional carboxymethyl cellulose sodium encapsulated phosphorus-enriched biochar composites: Multistage adsorption of heavy metals and controllable release of soil fertilization, Chem. Eng. J. 453 (2023).